Journal of Materials and Environmental Science
ISSN : 2028-2508
CODEN : JMESCN

J. Mater. Environ. Sci., 2020, Volume 11, Issue 5, Page 808-822

http://www.jmaterenvironsci.com

Preparation and Characterisation of Titanium Carbide Thin Films for Surface Brillouin Scattering studies

C. Sumanya [1], D M. Wamwangi [2,3], J D. Comins [2,3]

[1] *Institute of Material Sciences, Processing and Engineering Technology, Chinhoyi University of Technology, Zimbabwe*
[2]*DST/NRF Centre of Excellence in Strong Materials, University of Witwatersrand, Johannesburg, WITS 2050, South Africa*
[3]*Materials Physics Research Institute, School of Physics, University of Witwatersrand, Johannesburg, WITS 2050, South Africa*

Received 07 Jan 2020,
Revised 03 May 2020,
Accepted 04 May 2020

Keywords
- ✓ Titanium Carbide films,
- ✓ Preparation and Characterisation,
- ✓ Surface quality,
- ✓ Surface Brillouin scattering.

csumanya@cut.ac.zw;
Phone: +263784741898;

Abstract

TiC films, on both (100) single crystal silicon and 6H (0001) silicon carbide substrates with various thicknesses were synthesized using RF magnetron sputtering. Films were prepared at 6×10^{-3} mbars (0.6 Pa) with no substrate heating. Emphasis was given on optimising the quality of films for surface Brillouin scattering (SBS) studies. The films were characterized by X-ray reflectometry (XRR), glancing incidence X-ray diffraction (GIXRD) and X-ray photoelectron spectroscopy (XPS) to assess the quality of the films for surface Brillouin scattering (SBS) studies. Sputter rates were deduced for different powers. Density and roughness of the films were measured using XRR. GIXRD measurements showed that there was no preferential orientation for the films prepared at different powers. Only a random distribution of crystallites was observed. Stoichiometry of the TiC films were verified by XPS measurements.

1. Introduction

Properties of deposited titanium carbide (TiC) films depend strongly on the deposition method and conditions. There are many methods used to deposit TiC films such as chemical vapour deposition (CVD),[1-4] pulsed laser deposition (PLD) [5-6] and physical vapour deposition (PVD [7-9]. One major advantage of PLD and PVD processes is that compound films can be prepared at low substrate temperatures [10-11]. This is especially convenient in order to preserve the bulk properties of the substrate during the deposition process. Usually CVD methods are limited owing to high temperatures involved during the process.

PVD processes are divided into evaporation and sputtering. In evaporation, atoms are removed from the source by thermal means, whereas in sputtering, surface atoms are removed from a target material by the interaction of incident particles and ions of a gas. The deposition of thin films by sputtering involves the acceleration of ions in many cases from gaseous (inert gas) plasma to bombard a negatively biased target material. The thin films in the present work were prepared using the sputtering method.

Sputtering was first observed in a dc gas discharge tube by Grove in 1852 [12] and five years later Faraday produced thin films using the evaporation method [13]. Sputtering allows the deposition of thin films with the same composition as the target source. This is the primary reason for its widespread

use in the deposition of metal alloy systems [14-16]. The sputtering process can be divided into three categories, namely; direct current (DC) sputtering, radio frequency (RF) magnetron and reactive sputtering. However, there is variance within each category (e.g. DC bias) and hybrids between categories (e.g. reactive RF). In this work TiC thin films were synthesized using RF magnetron sputtering and characterized by X-ray reflectometry (XRR), glancing incidence X-ray diffraction (GIXRD) and X-ray photoelectron spectroscopy (XPS) to assess the quality of the films for surface Brillouin scattering (SBS) studies.

2. Importance of surface quality in SBS studies

SBS allows surface acoustic excitation in the GHz frequency range to be studied, and hence permits the elastic properties of a material to be determined. The particle displacement of surface waves decays exponentially beneath the surface, extending on the order of a wavelength into the bulk. The elastic properties studied by SBS are therefore associated with the region within a few hundred nanometres of the surface and can differ with those of the bulk. There are a number of reasons attributed to these variations. Among which includes the near surface damage caused by polishing or ion bombardment, surface roughness or impurities in the form of surface films.

2.1 Surface damage due to polishing

Mendik et al.,[17] showed that the surface damage caused by polishing a nickel single crystal resulted in lower measured surface acoustic wave (SAW) velocity as compared to theoretical values. There was a roughly 6% decrease of the measured SAW velocities as compared to those calculated from bulk elastic constants. However scanning acoustic microscopy (SAM), which probes much greater depth than SBS, gave velocities comparable to the calculated values. To improve the SBS results, the samples where sputtered and annealed so as to reduce the amount of surface damage. They reported a 3% increase in the SBS velocities, while the SAM results showed hardly any change.

2.2 Surface roughness

It is found that the surface roughness of samples is crucial for the successful measurement of surface acoustic modes. Smooth or polished surfaces produce less elastic scattering of light and thereby enhance the detection of weak inelastic scattering peaks in the Brillouin spectrum.

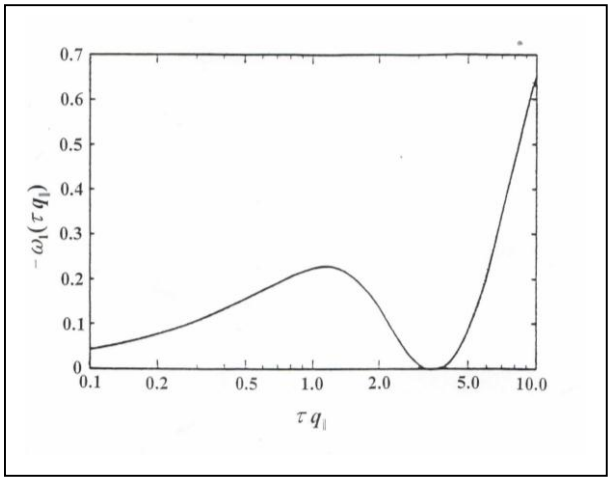

Figure 1: Rayleigh frequency shift due to surface roughness as a function of $\tau q_{\parallel}$ (*After Eguiluz and Maradudin [18]).*

Eguiluz and Maradudin [18] showed theoretically that surface roughness not only attenuates surface waves but also decreases their frequency $\omega(q_{\parallel}) = vq_{\parallel}$, where $q_{\parallel}$ is defined as the surface wave vector component parallel to the surface and v is the velocity. The shift in frequency $\omega_1(q_{\parallel})$ can be written conveniently in the form

$$\frac{\omega_1(q_\parallel)}{\omega(q_\parallel)} = (\delta/\tau)^2\,\omega_1(\tau q_\parallel)\,, \qquad (01)$$

where δ is the root mean square (roughness) departure of the surface from flatness and τ is the average distance between peaks and valleys in the rough-surface profile. In Eq. (01) it is seen that the ratio of the frequency shift $\omega_1(q_\parallel)$ and the frequency $\omega(q_\parallel)$ of a Rayleigh wave propagating on a flat surface is given by the product of the "universal" function $\omega_1(\tau q_\parallel)$ and the $(\delta/\tau)^2$ ratio which describes the rough-surface profile. The "universal" function $\omega_1(\tau q_\parallel)$ relates the frequency shift of a surface wave to the scale of the surface roughness. Fig. 1 shows the frequency shift of a Rayleigh wave due to surface roughness as a function of the product $\tau q_\parallel$. In summary, any imperfections on the surface region e.g., dislocations, pores and micro cracks contribute to a decrease in SAW velocities measured by SBS and an increase in the elastically scattered light. In this work, no polishing of the film surface was necessary as very smooth surfaces were produced. The roughness of the films were measured by the XRR technique as discussed in Section 4.2.

2.3 Impurities in the form of surface films

A native oxide layer on the surface of a film or substrate will inevitably shift the frequency of the SAW. If we take silicon as an example, it is known that commercial silicon supports a native oxide layer of about 2 nm thick [19]. Hence this will have an effect on the measured SAW velocity. In the case of substrates, a useful practice is to sputter etch the substrates prior to deposition so as to remove the oxide layer. However, little can be done if the material deposited has a high affinity for oxygen. The substrates used in the present work were sputter etched for 5 minutes prior to deposition.

3. Film preparation

3.1 RF magnetron sputtering

Magnetron sputtering can be done in either DC or RF modes. In RF magnetron sputtering, a radio frequency (RF) signal superimposed on a target self-bias (usually negative) is used to ionize the inert gas. This will generate a self sustained glow discharge constituting mainly of positive gas (argon) ions. The schematic diagram of the entire sputtering process is shown in figure 2. The magnets located behind the targets are used to increase the percentage of electrons that take part in ionisation events. This will increase both the probability of electrons striking the argon atoms and the length of electron path and hence increase the ionisation efficiency significantly.

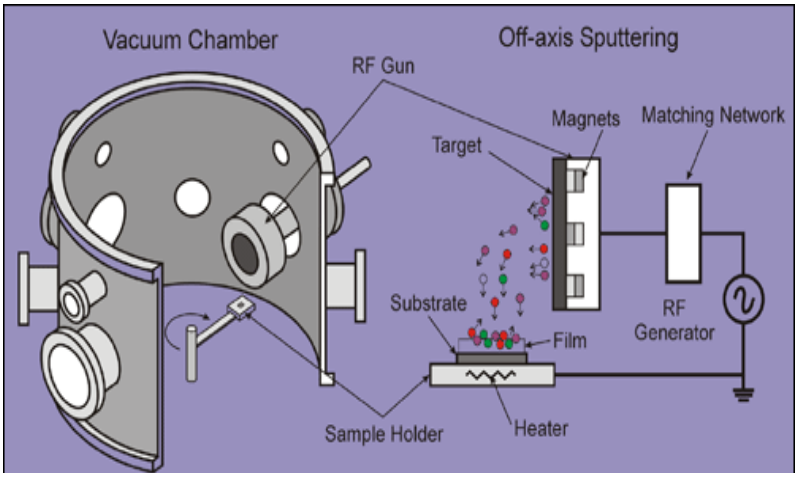

Figure 2*:* Schematic diagram of RF sputter system with the sputtering process shown adjacent thereto *(after www.phasis.ch)*.

The negative potential difference between the target (biased negatively) and the plasma, extracts Ar^{2+} ions from the plasma and accelerates them onto the target. The surface atoms of the target are ejected

by momentum transfer and are deposited as thin films into the surface of the substrate. Sputter yield, *S*, is defined as the mean number of atoms removed from the surface of solid per incident ion. The sputter yield is a process parameter that is influenced by the RF power, gas pressure and target material.

Sputtering has no limitation regarding target materials and both pure metals and insulators can be grown as deposited films. For insulators an RF power supply is needed in order to avoid charge build-up on the target surface [20]. The presence of a matching network between the RF generator and the target is necessary in order to optimize the power dissipation in the discharge.

3.2 Experimental procedure

TiC films, on both (100) single crystal silicon ($\approx 15\times15\times0.5$ mm^3) and 6H (0001) silicon carbide ($\approx 4\times4\times1$ mm^3) substrates, with various thicknesses were deposited using the RF magnetron sputtering apparatus in the School of Physics of the University of the Witwatersrand, Johannesburg. All substrates were ultrasonically cleaned with methanol prior to being loaded into the deposition chamber. The system was evacuated with a fore- and turbo-pump to a base pressure of around 10^{-6} mbar prior to thin film deposition. Such a high vacuum was essential to prohibit target poisoning or contamination or formation of an N_2 / O_2 monolayer during deposition. A water-cooled stoichiometric titanium carbide target was used for the deposition of TiC on to a substrate located at 60 mm from the target. The purity grades of the materials involved were 99.9 *wt*.% for titanium carbide and 99.997 *vol*.% for argon. The target was sputter-cleaned prior to each deposition for 5 minutes at a power of 250 W. The silicon substrates were etched with very low energy (40 W) for 5 minutes in Ar prior to deposition in order to remove the native oxide layer from the substrate surface. All the films characterized in this work were prepared under similar conditions at an Ar working gas pressure of 6×10^{-3} mbar. A specially designed substrate holder was used for silicon carbide substrates due to their small size ($\approx 4\times4\times1$ mm^3). The substrate holder carries up to 7 substrates and it is equipped with a shutter system to ensure single substrate exposure to the target and plasma during deposition. The thickest intended film layer is deposited first over the entire surface followed by appropriate movement of the shutter to the next substrate. This procedure is continued in an undisturbed manner for each of the 7 films with various thicknesses ranging from 50 nm to 800 nm which were to be used for SBS measurements.

4. Film characterisation

4.1 Film thickness

Film thickness is a critical parameter that must be determined accurately in order to obtain dispersion relations for diverse thin film - substrate configurations such as, the TiC/Si or TiC/SiC combination. For film thickness and deposition rate measurements, two sets of TiC films on silicon were prepared using RF magnetron sputtering. Each set comprised of five thin films prepared at powers of 50W, 100W, 150W, 200W, and 250W. The substrates ($\approx 15\times15\times0.5$ mm^3) from each set were cut from a separate silicon wafer (diameter ≈ 75 mm) and ultrasonically cleaned for each deposition run. To obtain the film thickness, two parallel lines were marked closely to each other at the centre of the substrates using a sharp non-permanent marker. The region covered by the ink provided weak adhesion to the film and could be removed using any organic solvent. All depositions were carried out for 60 minutes to allow sufficient deposition at low powers. After the deposition, the films were immersed in alcohol/acetone to etch away the masked potions of the thin film thereby yield a doubly step edged thin film at the centre of the substrate (Fig. 3). Two step edges were preferred to define unambiguous baseline for accurate film thickness determination using a surface profilometry. A profilometer (Dectak Alphastep 5000 provided by DENEL dynamics, South Africa) was used to scan the step for film thickness determination due to the following reasons:

- a high lateral resolution extending up to 5 mm,
- a high accuracy and precision especially for thin films with thickness > 100 nm.

Figure 4 below shows a typical layer thickness measurement for a TiC layer on (100) Si prepared at 200W

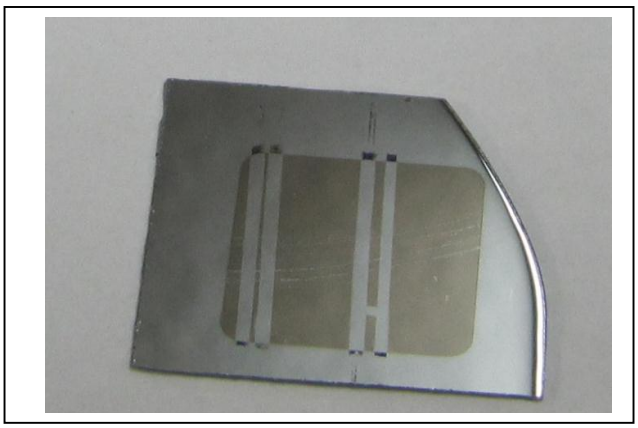

Figure 3: A sample of TiC thin film on silicon substrate after immersion in alcohol, showing clearly the two step edges.

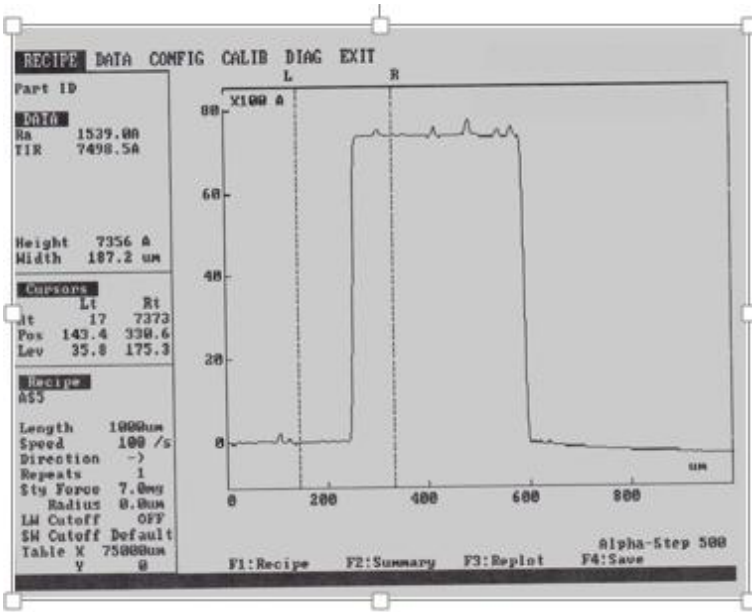

Figure 4: Profilometer measurement for a film prepared at 200 W showing a layer thickness measurement of 736 nm.

Table 1: Deposition rates at different powers for TiC films

Power (W)	Set A Thickness (nm)	Set B Thickness (nm)	% Deviation	Average Thickness (nm)	Sputter Rate (nm min^{-1})
50	92	100	-8.7	96.0	1.6
100	327	320	2.1	323.5	5.4
150	543	537	1.1	540.0	9.0
200	731	736	-0.7	733.5	12.2
250	805	801	0.5	803.0	13.4

Table 1 presents profilometer results for the two sets at different powers. Film thickness measurements between the two sets are in good agreement as evident from percentage deviation values. The deposition rates for different powers are deduced from Table 1 by taking the average of Set A and Set B. Since ion bombardment energy strongly depends on RF power and the sputtering yield is proportional to the ion bombardment energy, it follows that the sputter rate must strongly depend on the RF power. Table 1 confirms that the sputter rate increases with increasing RF power. Fig 5 shows the relationship between

layer thickness and RF power. It can be concluded that there is a linear relationship between the layer thickness and applied power up to 200 W. The behaviour of the deposition rate beyond 200 W was not established since 250 W was the maximum power which could be used with the available RF generator. From these measurements, it was decided to use a power of 200 W (the highest giving linear deposition rate). This power corresponds to a deposition rate of 12.2 nm min^{-1}.

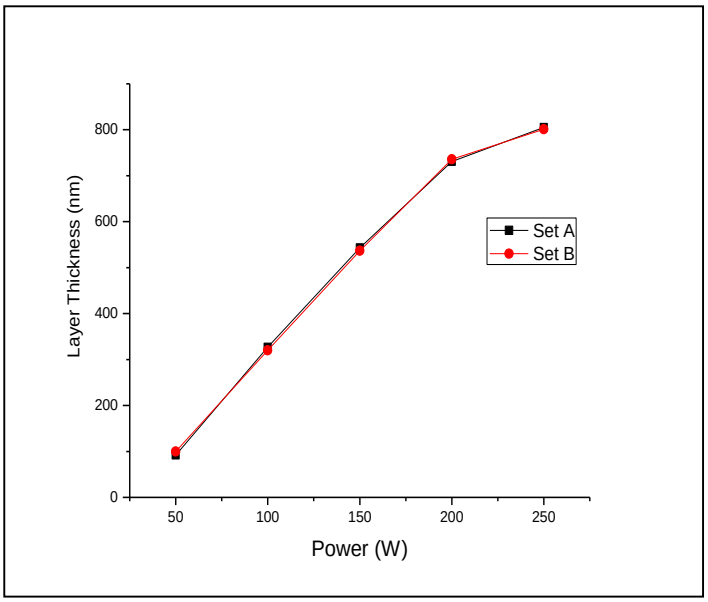

Figure 5*:* Graph of layer thickness against power. Points are joined as a guide to the eye, not as the best fit.

4.2 X-Ray reflectometry (XRR)

XRR is a non-destructive and non-contact technique used for the determination of thickness, density and roughness of films with high precision. The technique involves monitoring the intensity of the X-ray beam reflected by the specimen at grazing angles usually less than 5° in the incident angle. A thorough description of XRR can be found elsewhere [21-24].

In principle a monochromatic X-ray beam of wavelength λ irradiates a sample at a grazing angle θ_R and the intensity reflected at an angle $2\theta_R$ is recorded by a detector. Total reflection will occur at or below a certain angle, θ_c – the critical angle. The angle varies depending upon the electronic density of the material. For ideal flat surface the reflectivity decreases at angles above the critical angle in proportion to θ_R^{-4}. If the material surface is rough, a more drastic decrease in reflectivity occurs. This is because roughness gives rise to diffuse scattering, resulting in less intensity in the specularly reflected beam. Given a thin film evenly overlaid on the substrate with electronic density different from the substrate, the reflected X-rays from the interface between the substrate and the thin film as well as from the free surface of the thin film will interfere constructively and destructively. The period of the interference fringes and the fall in the intensity are related to the thickness and the roughness of the layer. As a result density (ρ), film thickness (d), and roughness ($\sigma\, rms$) may be extracted from the critical angle, interference spectra, and reflectivity. The following discussion follows closely the treatment of Bontempi *et al*. [25] At X-ray frequencies, the refractive index, n, can be expressed as:

$$n = 1 - \delta - i\beta, \qquad (02)$$

$$\text{where} \quad \delta = \frac{\rho_e r_e \lambda^2}{2\pi}, \qquad (03)$$

$$\beta = \frac{\mu\lambda}{4\pi}, \qquad (04)$$

ρ_e is the electron density, r_e is the classical electron radius = e^2/mc^2, λ is the X-ray wavelength and μ is the linear absorption coefficient for energies far from X-ray threshold. From the measurement of the critical angle, the density of the film can be estimated by the formula

$$\theta_c = \sqrt{2\delta} = \lambda\sqrt{\frac{r_e\rho_e}{\pi}}\,. \qquad (05)$$

For incident angles greater than θ_c ($\theta_R > \theta_c$) the X-ray beam penetrates inside the film. Reflection will therefore occur at the top and bottom surfaces of the film. The interference between the rays reflected from the top and the bottom of the film surfaces results in interference fringes. For intensity maxima, the path difference between the reflected waves should be an integral multiple of the incident wavelength,

$$m\lambda \approx 2d\sqrt{\sin^2\theta_m - \sin^2\theta_c}\,, \qquad (06)$$

where *m* is an integer. Since the angles are small, equation (06) can be expressed as

$$m\lambda \approx 2d\sqrt{\theta_m^2 - \theta_c^2}\,. \qquad (07)$$

The layer thickness is therefore given by $d = \frac{1}{2}m\lambda\frac{1}{\sqrt{\theta_m^2 - \theta_c^2}}$. (08)

For very small angles ($\theta_R < 0.2^o$), the scattered X-ray intensity is almost constant, whereas above the critical angle the intensity rapidly drops by several orders of magnitude and oscillations appear in the spectrum. These oscillations are called Kiessig fringes .[25] The presence of surface roughness decreases the specular intensity of the whole curve progressively and interface roughness gives rise to progressive damping of the Kiessig fringes.

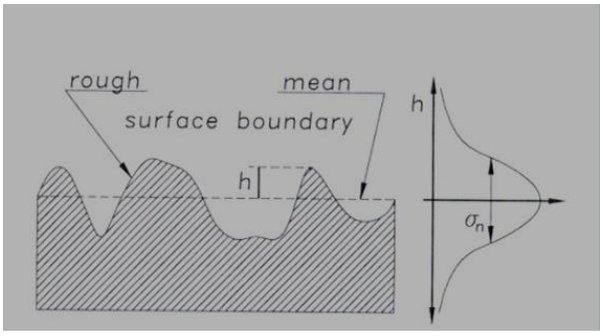

Figure 6: Interface roughness according Névot and Croce [26]. The roughness of the interface is described using the Gaussian function (*after Filies* et al) [27].

Surface or interface roughness can be obtained, by a refinement of the experimental data with algorithms put forward by Névot and Croce . They considered roughness by assuming non-homogeneous thickness. They assumed that the rough interface may be estimated by a Gaussian distribution of peaks and valleys with a mean *d* (layer thickness) and a standard deviation σ_n (Fig. 6).
Thus, the roughness coefficient may be calculated as

$$\zeta_n = \exp\left(-8\frac{\sigma_n^2}{\lambda^2}f_n f_{n-1}\right), \qquad (09)$$

where f_n are the Fresnel factors for the *n*th interface [27]

The XRR method gives accurate measurements for layer thicknesses, *d*, of less than 200 nm. Three samples of TiC films ($d \leq 200$ nm) on Si(100) substrates were prepared using RF magnetron sputtering at 100 W, 200 W and 250 W for 28 min, 14 min and 13 min, respectively for XRR measurements. The corresponding layer thicknesses of 151.2 nm, 170.8 nm and 174.2 nm, respectively, were extracted from the deposition rates of Table 1.

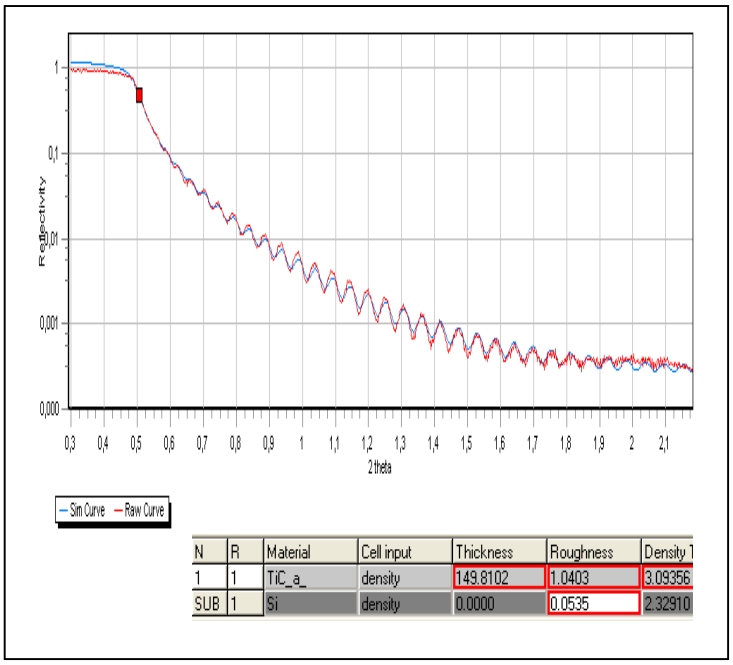

N	R	Material	Cell input	Thickness	Roughness	Density T
1	1	TiC_a_	density	149.8102	1.0403	3.09356
SUB	1	Si	density	0.0000	0.0535	2.32910

Figure 7: XRR measurement for a TiC film on silicon prepared at 100 W for 28 min. The fit parameters for the simulation curve are highlighted in red. The parameter values are: layer thickness 149.81 nm, roughness 1.04 Å and density 3.09 g/cm^3

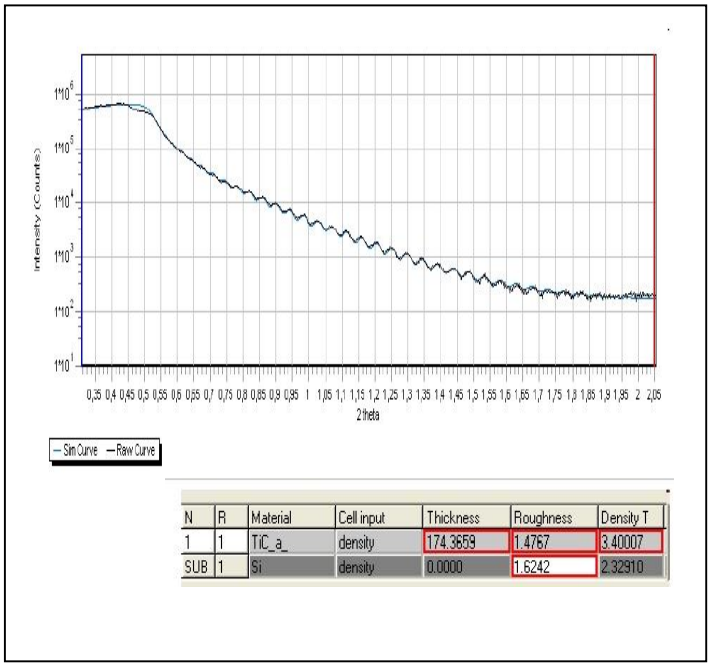

N	R	Material	Cell input	Thickness	Roughness	Density T
1	1	TiC_a_	density	174.3659	1.4767	3.40007
SUB	1	Si	density	0.0000	1.6242	2.32910

Figure 8: XRR measurement for a TiC film on silicon prepared at 200 W for 14 min. In this figure the y–axis is given as intensity in arbitrary units instead of the normalised reflectivity. The fit parameters for the simulation curve are highlighted in red. The parameter values are; layer thickness 174.37 nm, roughness 1.48 Å and density 3.40 g/cm^3.

A Bruker New D8 Discover X-ray diffractometer was used for all the XRR measurements. Figures 7 and 8 show XRR results for films deposited using RF magnetron sputtering at 100 W and 200 W, respectively.

Table 2: XRR results for TiC films prepared at 100 W, 200 W and 250 W

Power (W)	Density (g/cm^3)	Roughness (Å)	XRR Thickness values (nm)	Profilometer Thickness values (nm)	Deviation
100	3.09	1.04	150	151	-1%
200	3.40	1.48	174	171	2%
250	3.63	0.72	172	174	-1%

There is a steady increase in the density of the films with increase in the RF power but it remains less than that of bulk TiC, which is 4.9 g/cm^3 [28]. The increase in film density is attributed to increase in adatom surface energy with RF sputter power which enhances thin film compactness. The roughness of the films remains low regardless of the RF power and the layer thickness values are in good agreement with values measured using the profilometer. Density and layer thickness values are useful in the calculation of theoretical SBS spectra [29]. Low roughness values imply that less elastic light will be observed in SBS measurements. This will enhance the detection of weak inelastic scattering peaks [29].

4.3 Glancing incidence X-ray diffraction (GIXRD)

In a GIXRD experiment, an X-ray beam is directed onto the surface of the film at an incident angle (α_d) of 1^o or less and the detector is placed in a horizontal plane, parallel to the film surface to record diffraction from lattice planes which are perpendicular to the surface (Fig. 9).

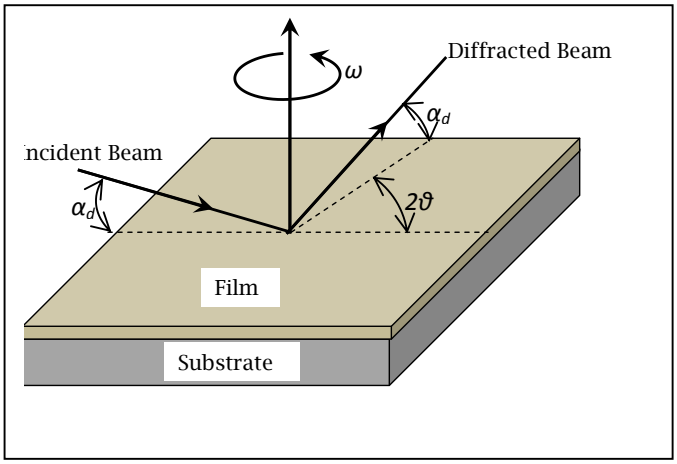

Figure 9: Schematic diagram of the GIXRD geometry.

Radial ($2\theta_d$) scan and/or angular (ω) scan methods can be used to collect GIXRD data. In a radial scan, both the film and the detector are scanned to record diffraction along a fixed direction on the substrate while in an angular scan the detector is stationary at a fixed $2\theta_d$ angle, while the film rotates about its surface normal to record in-plane diffraction from lattice planes which have fixed lattice spacing [30-31]. TiC films of 180 nm layer thickness were grown by RF magnetron sputtering on (001) silicon substrates, for this measurement. The films were prepared at 100 W, 150 W, 200 W and 250 W. A Bruker D8 Advance reflectometer equipped with a Göbel mirror was used for the measurements. A Göbel mirror comprises parabolically bent multilayers with a laterally graded period to achieve monochromatic and parallel X-ray beams [24-32].

The measurements were taken using a radial scan. The data were used to determine the orientation and crystallite size of the films. The incidence angle, α_d, was kept at a low value of 0.75^o in order to maximize the signals from the layers and minimize the substrate reflections. The measurements were performed for a $2\theta_d$ range of 30° to 90°. The measurements show that there is no preferential orientation for all samples. There is however a random distribution of crystallites. The identification of the (111), (200), (220) reflections (Fig. 10) is clearly attributive of the cubic TiC structure but their low intensities indicate an amorphous structure with randomly distributed crystallite grains. The peak at 80° for the

100 W and 250 W samples is not so clearly identified. From the identified peaks, the crystallite size can be roughly estimated to be 3 nm using the Scherrer equation [33] for all samples.

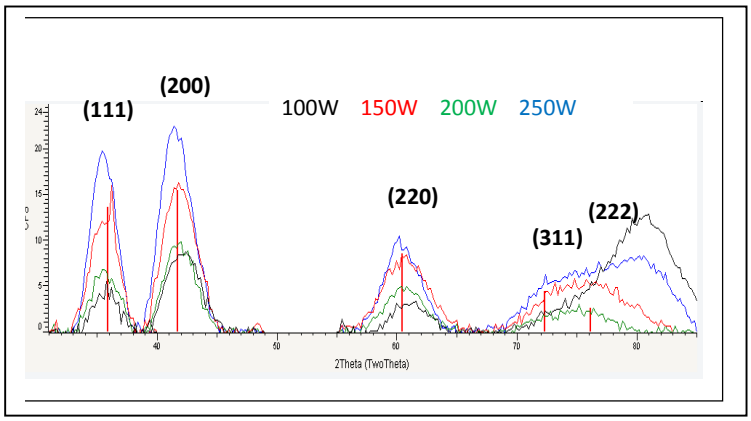

Figure 10: GIXRD measurements for TiC films prepared at 100 W, 150 W, 200 W and 250 W.

4.4 X-ray photoelectron spectroscopy (XPS)

X-ray photoelectron spectroscopy (XPS) can be used to determine the elemental composition, empirical formula, chemical state and electronic state of the elements that exist within a film. In order to verify the stoichiometry of TiC films, two samples of *TiC/Si* were analysed using XPS equipment (PHI 5000 Versaprobe – Scanning ESCA Microprobe) at the University of the Free State, South Africa. The two films of 488 nm and 732 nm thicknesses were deposited at 200 W. Figure 12 shows a typical XPS raster spectrum of the deposited TiC films. Ti, C, O, N and Ar-related peaks were clearly identified. From this survey spectrum, regions of interest were identified and high resolution C 1s, Ti 2p and O 1s XPS peaks were recorded.

Figures 12, 13 and 14 shows the XPS survey spectra for a 488 nm TiC film deposited on silicon showing clearly the C 1s, Ti 2p and O 1s peaks. Table 3 summarizes the assignments of the peaks with binding energies.

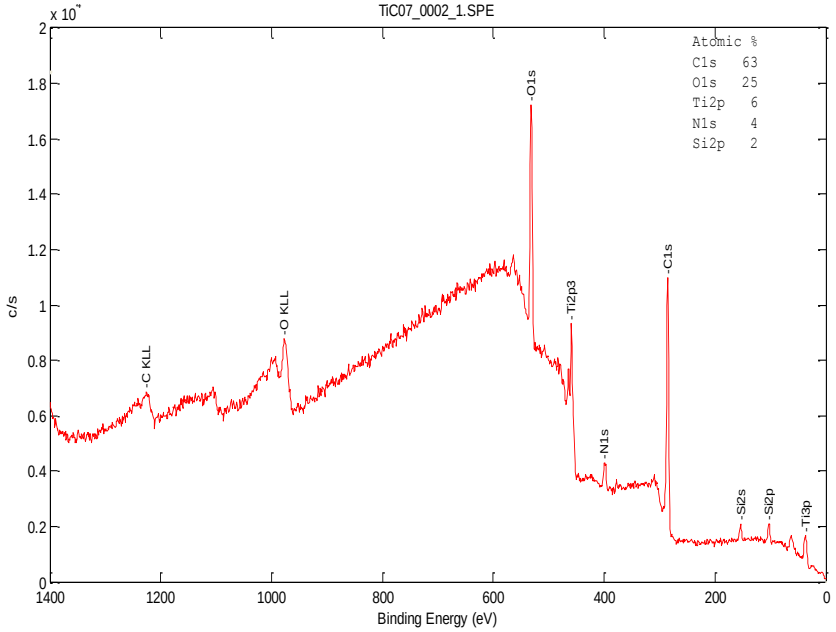

Figure 12: XPS survey on the unetched surface of a 488 nm TiC film deposited on silicon at 200 W. The atomic percentage of the elements at the surface are 63% C 1s, 25% O 1s, 6% Ti 2p, 4% N 1s and 2% for Si 2p.

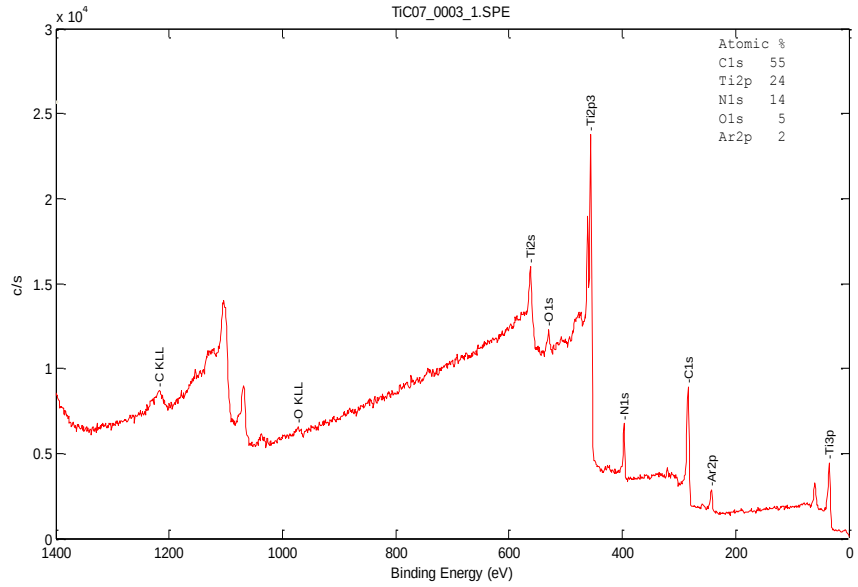

Figure 13: XPS survey spectrum of a 488 nm TiC film deposited on silicon at 200 W. This was obtained after sputter etching for 1 min. The atomic percentage of the elements are 55% C 1s, 24% Ti 2p, 14% N 1s, 5% O 1s, and 2% for Ar 2p.

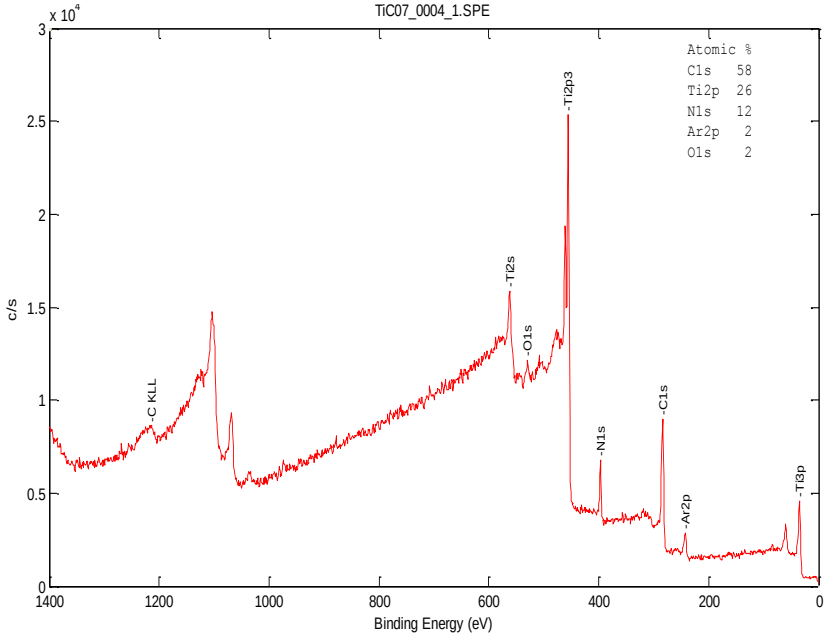

Figure 14: XPS survey spectrum of a 488 nm TiC film deposited on silicon at 200 W. This was obtained after sputter etching for 2 min. The atomic percentage of the elements are 58% C 1s, 26% Ti 2p, 12% N 1s, 2% O 1s, and 2% for Ar 2p.

XPS surveys were done with a 100 µm Al monochromatic X-ray beam at a power of 25 W and voltage of 15 kV. As for depth profiling, a 2 × 2 mm raster Ar ion gun was used at 2 kV with a current of 2 µA. The sputter rate was about 85 Å/min. The XPS survey on the surface (Fig. 12) shows a very strong oxygen signal (25% atomic percentage). This is reduced to 5% (Fig.13) after etching for 1 min and further reduced to 2% (Fig. 14) after etching for 2 min (≈170 Å deep). This shows that oxygen is predominantly at the surface of the films extending to a thickness of about 170 Å. There is however evidence that nitrogen is incorporating itself in the film as evident from a constant atomic percentage of 12% regardless of etching. All the films were prepared in an Ar pressure of 6 x 10^{-3} mbar, which explains the Ar peak. Other notable elements from the survey are C 1s and Ti 2p. High resolution spectra C 1s, Ti 2p, O 1s and N 1s are shown in figure 15. The analysis of the results was done by Prof H C Swart and his group at the University of Free State, South Africa. The results are tabulated in Table 3.

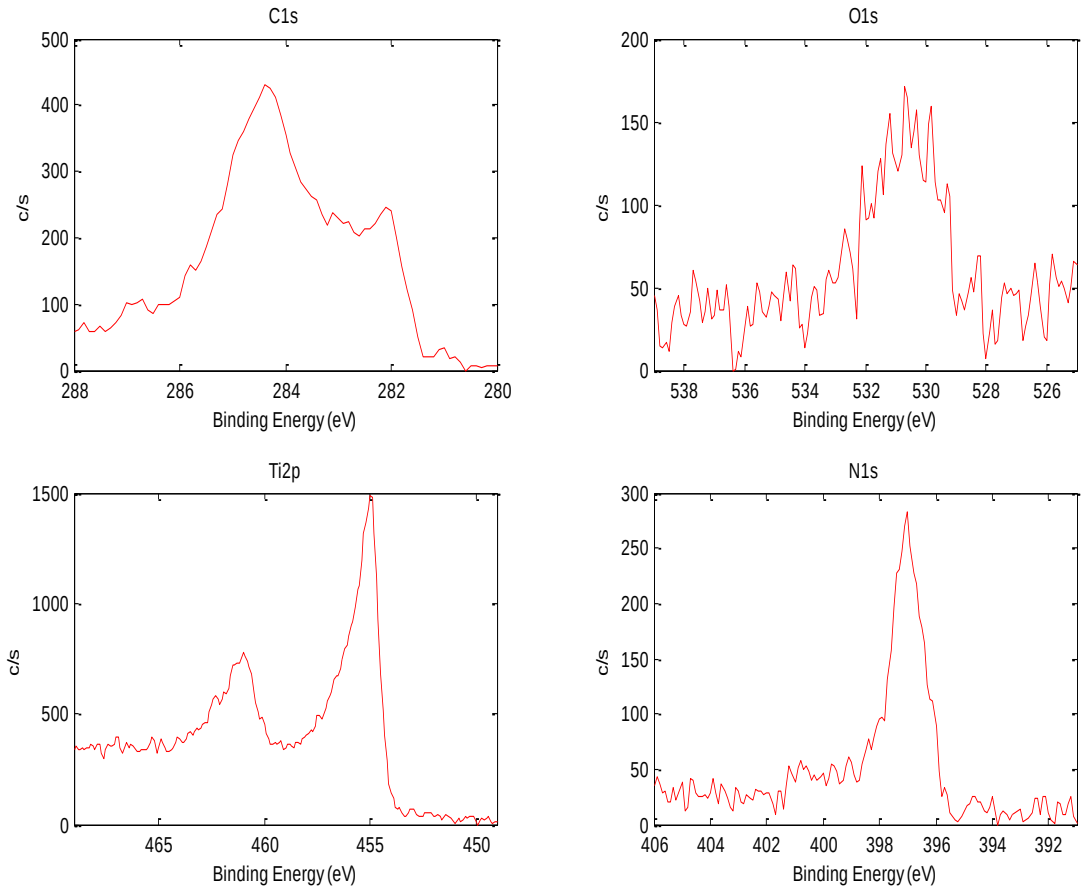

Figure 15: Magnified XPS spectra of C 1s, O 1s, Ti 2p and N 1s XPS spectra for a 488 nm TiC film.

Table 3**:** Deconvolution of C 1s, O 1s, Ti 2p and N 1s peaks [34] for the 488nm TiC film

Peak Position (eV)	**Description**
(a) Deconvolution of the C 1s peak	
282.5	TiC
284.3	C
285.4	C with N/C with O
(b) Deconvolution of the O 1s peak	
529.7	?/TiO_2/TiO
530.8	TiO
532.1	?
(c) Deconvolution of the Ti 2p peak	
455.1	TiC $2p_{3/2}$
455.2	TiO $2p_{3/2}$
458.4	TiO_2 $2p_{3/2}$
461.2	TiC $2p_{1/2}$
461.4	TiO $2p_{1/2}$
464.6	TiO_2 $2p_{1/2}$
(d) Deconvolution of the N 1s peak	
397	?TiN
399	?N with C/C_5H_5N

From the high resolution XPS spectra of the peaks (Fig. 15), it can be inferred that two major chemical compounds are present: the isolated carbon is represented by C 1s peak of 284.3 eV and TiC is represented by three peaks, C 1s peak of 282.5 eV, Ti $2p_{3/2}$ peak of 455.1 eV and Ti $2p_{1/2}$ peak of 461.2 eV. The oxygen and nitrogen peaks are inconclusive. Due to the very high chemical affinity of Ti for oxygen and nitrogen, these gases may incorporate into the TiC films during film deposition as a result of interactions with residual gases in the vacuum.

Conclusion

TiC films prepared by this technique were stoichiometric as evident from XPS measurements. After etching about 170 Å deep into the surface the measurements showed strong signals for TiC with minimal oxygen signals. Isolated nitrogen signals are also present in the films. Presence of oxygen at the surface and nitrogen in the film was attributed to the very high chemical affinity of titanium for these gases. Nitrogen gas is mainly used in breaking vacuum inside the deposition chamber; it is therefore not unexpected that this gas is detected in the film.

It has been shown that the sputter rate depends on the RF power. An RF power of 200 W was used for the preparation of films for SBS measurements. At this power the sputter rate was measured as 12.2 ± 0.1 nm min^{-1}. The densities and roughness of the films were measured using XRR. The measured density for films prepared at different RF powers was lower than the bulk density. This is expected since it is generally accepted that most deposition techniques create film densities which deviate from the bulk density [35-36]. The measured low roughness implies that the films were of high quality. Surface quality is very crucial in SBS measurements. Smooth surfaces produce less elastically scattered light which will enhance the detection of weak inelastic scattering peaks.

The crystallinity of a film is also an important aspect in the final performance of the coating. Crystallinity of hard coatings is directly correlated to the substrate temperature during deposition [37]. The higher the substrate temperature, the higher the crystalline order of the coating. Mani *et al*., 2005 [38] reported that the sputtering pressure had an influence on the substrate morphology and chemical composition of the TiC films prepared using RF sputtering. It was observed that the film structure gradually changed from a mixture of distorted TiC at lowest pressure, 0.35 Pa, to homogeneous TiC at higher pressure, 1 Pa, with preferential orientation [111]. Djafer *et al*., 2014 [39] confirmed preferential orientation in TiC films prepare with a substrate bias. However films prepared in this work were prepared at 6×10^{-3} mbars (0.6 Pa) with no substrate heating. GIXRD measurements showed that there was no preferential orientation for the films prepared at different powers. Only a random distribution of crystallites was observed. This is consistent with results reported by Mani *et al*., 2005 [38].

Pang (1997) [40] found that the general elastic properties of polycrystalline aggregate with random distribution of anisotropic crystallite of any symmetry classes are the same as those of isotropic materials. We can therefore conclude that only two non-independent elastic constants (isotropic case) can be determined for the TiC films in SBS studies instead of five effective elastic constants (polycrystalline aggregates with preferred orientation).

Acknowledgements - The authors thank the DST/NRF Centre of Excellence in Strong Materials (CoE-SM), South Africa for financial Support.

References

1. H. Asada, Y. Kishi, Y. Hirose, Measurement of Young's moduli of TiC-coated film by the X-ray method. *Thin Solids Films*, 236 (1993) 247-252 https://doi.org/10.1016/0040-6090(93)90678-I
2. Y. I. Konyashin, Thin TiCx, films chemically vapour deposited onto cemented carbides from the $TiC1_4$-CCl,-H_2 mixture. *Thin Solid Films*, 278 (1996) 37-44, https://doi.org/10.1016/0040-6090(95)08134-8

3. L. Guzman, M. Bonelli, A. Miotello, D. C. Kothari, (1998). Process parameters optimization for TiN and TiC formation using reactive ion beam assisted deposition. *Surf. Coat. Technol.*, 100/101 (1998) 500-502 https://doi.org/10.1016/S0257-8972(97)00679-8
4. L. K. Choy, Chemical vapour deposition of coatings. *Prog. Mater. Sci.*, 48 (2003) 57-170. https://doi.org/10.1016/S0079-6425(01)00009-3
5`. J. Tang, J. S. Zabinski, J. E. Bulman, TiC coatings prepared by pulsed laser deposition and magnetron, *Surf. Coat. Technol.* 91 (1997) 69-73. https://doi.org/10.1016/S0257-8972(96)03124-6
6. F. Santerre, M. A. Khakani, M. Chaker, J. P. Dodelet, Properties of TiC thin films grown by pulsed laser deposition. *Appl. Surf. Sci.*, 148 (1999) 24-33. https://doi.org/10.1016/S0169-4332(99)00139-7
7. R. Fillity, A. Perry, Residual stress and X-ray elastic constants in highly textured physically vapor deposited coatings. *Surf. Coat. Technol.*, 36 (1988) 647-659. https://doi.org/10.1016/0257-8972(88)90006-0
8. D. T. Quinto, Technology perspective on CVD and PVD coated metal-cutting tools. *Int. J. Refract. Met. Hard. Mater.*, 14 (1996) 7-20. https://doi.org/10.1016/0263-4368(96)83413-5
9. E. Kusano, A. Satoh, M. K. Nanto, A. Kinbara, Titanium carbide film deposition by DC magnetron reactive sputtering using a solid carbon source. *Thin Solids Films*, 343-344 (1999) 254. https://doi.org/10.1016/S0040-6090(98)01638-1
10. O. Rist, P. T. Murray, (1991). Growth of TiC thin films by pulsed laser evaporation. *Mater. Lett.*, *10* (7,8), (1991) 323-328. https://doi.org/10.1016/0167-577X(91)90146-W
11. U. Helmersson, M. Lattemann, J. Bohlmark, A. P. Ehiasarian, J. T. Gudmundsson, Review: Ionized physical vapor deposition (IPVD): A review of technology and applications. *Thin Solid Films*, 513 (2006) 1-24. https://doi.org/10.1016/j.tsf.2006.03.033
12. W. Grove, On the electro-chemical polarity of gases. *Phil. Trans. Roy. Soc.,Lond.*, 142 (1852) 87-101. https://doi.org/10.1098/rstl.1852.0008
13. M. Faraday, Experimental relations of gold (and other metals) to light. *Phil. Trans. R. Soc. Lond.*, 147 (1857) 145-181. https://doi.org/10.1080/14786445708642424
14. R. Berry, P. Hall, M. Harris, (1968) *Thin Film Technology*. (D. V. Nostrand, Ed.) Inc., Princeton.
15. W. Kiyotaka, S. Hayakawa, (1992) *Handbook of Sputtering Deposition Technology:principles,technology and applications*, Noyes Publications. Park Ridge, New Jersey.
16. D. Smith, (1995) *Thin Film Deposition: Principle and Practice.* McGraw-Hill Professional, New York.
17. M. Mendik, S. Satish, A. Kulik, G. Gremaud, P. Wachter, Surface acoustic wave studies on single-crystal nickel using Brillouin scattering and scanning acustic microscope. *J. Appl. Phys.*, 71 (1992) 2830-2834. https://doi.org/10.1063/1.351013
18. Eguiluz, A. G., and Maradudin, A. A. (1983). Frequency shift and attenuation length of a Rayleigh wave due to surface roughness. *Phys. Rev. B, 28*, 728. https://doi.org/10.1103/PhysRevB.28.728
19. J. Gotze, R. Mockel (2012) *Quartz: Deposits, Maineralogy and Analytics*, Springer Heidelberg, New York, Dordrecht
20. M. Ohring, (1992) *The Materials Science of Thin Films*, Academic Press, New York.
21. V. Holý, A. A. Darhuber, J. Stangl, G. Bauer, J. Nutzel, G. Abstreiter, Oblique roughness replication in strained SiGe/Si multilayers. *Phys. Rev. B*, 57 (19), (1998) 12435-12442. https://doi.org/10.1103/PhysRevB.57.12435
22. E. Bontempi, L. E. Depero, L. Sanagaletti, X-ray reflectivity and glancing-incidence diffraction from thin metallic Cr layers. *Phil. Mag. B, 80* (4), (2000) 623-633. https://doi.org/10.1080/13642810008209770
23. C. Schw, B. York, J. Marien, H. R. Blank, The use of X-Ray Reflectometry for single film thickness analysis in GMR multilayer stacks. *Advances in X-Ray Analysis*, 44 (2001) 295-301.

24. S. Kohli, C. D. Rithner, P. K. Dorhout, X-ray characterization of annealed iridium films. *J. Appl. Phys., 91* (3) (2002), 1149-1154. https://doi.org/10.1063/1.1429798
25. E. Bontempi, L. E. Depero, L. Sanagaletti, (2000). X-ray reflectivity and glancing-incidence diffraction from thin metallic Cr layers. *Phil. Mag. B,* 80 (4) (2000) 623-633. https://doi.org/10.1080/13642810008209770
26. L. Névot, P. Croce, Characterization of surfaces by the oblique reflection of x-rays: Application to the study of silicate glass polishing. *Rev. Phys. Appl. (Paris)* 15 (1980) 761-779 https://doi.org/10.1051/rphysap:01980001503076100
27. O. Filies, O. Böling, K. Grewer, J. Lekki, M. Lekka, Z. Stachura, B. Cleff, (1999). Surface roughness of thin layers-a comparison of XRR and SFM measurements. *Appl. Surf. Sci.,* 141 (1999) 357-365. https://doi.org/10.1016/S0169-4332(98)00524-8
28. K. E. Petersen, Silicon as a mechanical material. *Proceedings of the IEEE* , 70, (1982) *No 5*, 420-457. 10.1109/PROC.1982.12331
29. C. Sumanya, B. A. Mathe, J. D. Comins, A. G. Every, M. Osawa, H. Harada *J. Appl. Phys.,* 116 (2014) *133511* https://doi.org/10.1063/1.4896843
30. B. K. Agarwal, (1979). *X-Ray Spectroscopy-An introduction.* Springer, New York.
31. A. Segmülar, Characterization of epitaxial thin films by x-ray diffraction. *Mat. Sci. Forum* 79 (1991) 493-502 https://doi.org/10.1116/1.577259
32. M. Schuster, H. Göbel, Parallel-beam coupling into channel-cut monochromators using curved graded multilayers. *J. Phys. D: Appl. Phys.,* 28 (1995) A270.
33. B. D. Cullity, (1978). *Elements of X-Ray Diffraction* (2 ed.). Addison-Wesley, New York.
34. J. F. Moulder, W. F. Stickle, P. E. Sobol, K. D. Bomben, (1995). *Handbook of X-Ray Photoelectron Spectroscopy: A Reference Book of Standard Spectra for Identification and Interpretation of XPS Data.* (J. F. Moulder, & J. Chastain, Eds.) Perkin-Elmer Corporation (Physical Electronics).
35. Gürtler, K., Bange, K., Wagner, W., Raunch, F., and Hantsche, H. (1989). Characterisation of Ta_2O_5 layers by electron spectroscopy for chemical analysis Rutherford backscattering spectrometry, nuclear reaction analysis and optical methods. *Thin Solid Films, 175*, 185-189. https://doi.org/10.1016/0040-6090(89)90826-2
36. M. Hüppauff, K. Bange, B. Lengeler, Density, thickness and interface roughness of SiO_2, TiO_2 and Ta_2O_5 films on BK-7 glasses analysed by X-ray reflection. *Thin Solid Films* , 230 (1993) 191-198. https://doi.org/10.1016/0040-6090(93)90514-P
37. E. Portolan, C. L. Amorin, G. V. Soares, C. Aguzzoli, C. A. Perottoni, I. J. R. Baumvol, C. A. Figueroa, Carbon occupancy of interstitial sites in vanadium carbide films deposited by direct current reactive magnetron sputtering. *Thin Solid Films,* 517 (2009) 6493-6496. https://doi.org/10.1016/j.tsf.2009.03.202
38. A. Mani, P. Aubert, F. Mercier, H. Khodja, C. Berthier, P. Houdy, Effects of residual stress on the mechanical and structural properties of TiC thin films grown by RF sputtering. *Surf. Coat. Techn.,* 194 (2005) 190-195. https://doi.org/10.1016/j.surfcoat.2004.06.017
39. A. Z. A. Djafer, N. Saoula, N. Madaoui, A Zerizer, Deposition and characterization of titanium carbide thin films by magnetron sputtering using Ti and TiC targets. *Applied Surface Science,* 312 (2014) 57-62. https://doi.org/10.1016/j.apsusc.2014.05.084
40. Pang, W. (1997). *Measurement of Elastic Properties of Hard Films Using Brillouin Scattering.* PhD Thesis, University of the Witwatersrand, Johannesburg.